

Project No. 09-764

# An Innovative and Advanced Coupled Neutron Transport and Thermal Hydraulic Method (Tool) for the Design, Analysis and Optimization of VHTR/NGNP Prismatic Reactors

---

**Reactor Concepts RD&D**

**Dr. Farzad Rahnema**  
Georgia Institute of Technology

**In collaboration with:**  
Idaho National Laboratory

Madeline Feltus, Federal POC  
Abderrafi Ougouag, Technical POC

## NEUP PROJECT FINAL REPORT

**Project Title:** An innovative and advanced coupled neutron transport and thermal hydraulic method (tool) for the design, analysis and optimization of VHTR/NGNP prismatic reactors

**Covering Period:** October 1, 2009 through September 30, 2013

**Date of Report:** November 30, 2013

**Recipient:** Georgia Institute of Technology  
770 State Street NW  
Atlanta, GA 30332-0425

**Award Number:** DE-AC07-O5ID14517

**Project Number:** 09-764

**Principal Investigator:** Farzad Rahnema,  
Phone: 404-894-3731  
Email: [farzad@gatech.edu](mailto:farzad@gatech.edu)

**Collaborators:** Dingkang Zhang, Georgia Institute of Technology, [dingkang.zhang@gatech.edu](mailto:dingkang.zhang@gatech.edu)  
Abderrafi Ougouag, Idaho National Laboratory, [Abderrafi.Ougouag@inl.gov](mailto:Abderrafi.Ougouag@inl.gov)  
Srinivas Garimella, Georgia Institute of Technology, [sgarimella@gatech.edu](mailto:sgarimella@gatech.edu)

## SUMMARY

The objective of the project was to develop a 3-D advanced coarse mesh transport (COMET) method (tool) for steady-state and transient analyses in advanced VHTR/NGNP reactors. The project has led to a coupled neutronics and thermal hydraulic (T/H) core simulation tool with fuel depletion capability.

Current advancements in reactor core design are pushing VHTR/NGNP reactors toward greater core and fuel heterogeneity for the purpose of pursuing higher burn-ups, efficiently transmuted used fuel, maximizing energy production and improving plant economics and safety. As a result, an accurate and efficient neutron transport, with capabilities to treat heterogeneous burnable poison effects, is highly desirable for predicting the neutronics performance of the VHTR/NGNP reactors. The primary objective of the project was to advance the state-of-the-art for reactor analysis. The computational tool (COMET-Hex) has been developed in hexagonal geometry as an extension to an existing tool (COMET) for light and heavy water reactor analysis (in Cartesian geometry). The new method is based solely on transport theory without (spatial) homogenization in complicated 3-D geometries including control material. In addition to the hexagonal geometry extension, three additional capabilities have been developed concurrently by collaborators to increase the versatility of the code as an advanced and robust core simulator for VHTR/NGNP reactors. First, a depletion method within the core simulator has been developed and implemented. Secondly, the project has developed an elementary (proof-of-concept) 1-D time-dependent transport method for efficient transient analyses. The third capability has been to develop a thermal hydraulic method coupled to the neutronics transport module for VHTR/NGNP reactors.

## **I. PROJECT OVERVIEW**

### **Objective**

This objective of this project has been to develop a 3D, advanced coarse mesh transport method (COMET-Hex) for steady-state and transient analyses in advanced very high-temperature reactors (VHTRs). The project includes a coupled neutronics and thermal hydraulic (T/H) core simulation tool with fuel depletion capability.

### **Background:**

Theoretical modeling of steady-state and transient neutronics and thermal hydraulics behaviors has been an essential partner with experiment in designing, analyzing and optimizing VHTR/NGNP reactors. While many progresses have been made in this direction, there remain a variety of the most challenging areas where success has remained elusive.

Advanced reactor core designs for the VHTR/NGNP project are likely to include a large degree of heterogeneity and complexity, which will require much more effective and robust neutronics and thermal hydraulics modeling than is currently in use for most reactor systems. The traditional steady-state calculation scheme for light water reactors consists of three steps: (1) a series of detailed transport calculations using infinite-medium (specular reflective) boundary conditions (i.e., infinite medium assembly calculations) are performed for each unique assembly (or “colorset”) in the core; (2) spatially homogenized and energy collapsed cross sections are produced by flux-weighting the fine group or continuous energy cross sections, using the flux solution from the infinite medium assembly calculation; (3) the homogenized/collapsed parameters are used in a coarse-mesh, few-group nodal diffusion core calculation.

The extension of this approach to VHTR/NGNP reactors seems inadequate for a number of reasons. Firstly, neutron flux and fission density in the core are calculated using low-order techniques, such as diffusion theory, which rely on an assumption of linear anisotropy in the angular distributions through improved definitions of the diffusion coefficient. This assumption breaks down, and better techniques are required in regions with strong absorption, near material discontinuities, in fast energy groups and in general in (spatial and energy) regions where the flux gradient is sharp. Secondly, the lack of detailed (within assembly) solution because of the homogenization leads to the need for gross approximations in the reconstruction of the fuel pin power distribution. Generally, ad hoc methods, such as modulating the infinite medium assembly solution with the homogeneous solution from the core calculation, are used to obtain this distribution. In the absence of a new efficient whole-core transport code, these problems will remain unsolved for the foreseeable future.

In an effort to overcome the limitations of the conventional low-order techniques, a heterogeneous coarse mesh transport (COMET) method (tool) for steady-state and transient analyses of VHTR/NGNP reactors has been developed in this project. The detailed description of each task can be found in section III.

### **Products:**

The products developed as a result of this project are listed below:

- (1) A heterogeneous coarse mesh transport method/code for whole core calculations in 3-D hexagonal geometry for VHTR/NGNP prismatic reactors. This tool will be based solely on transport theory and will not require the homogenization of physics data within each coarse mesh. The proposed method will have the same accuracy and geometric flexibility as Monte Carlo methods and be significantly faster than the current fine mesh transport methods.

- (2) A depletion capability in COMET.
- (3) A 2-D thermal hydraulics module coupled to the neutronics transport module
- (4) A new set of 2-D and 3-D benchmark problems for VHTR/NGNP prismatic reactors

## II. PUBLICATIONS

This section lists the publications that resulted from this project.

### Journal papers:

1. Z. Zhang, F. Rahnema, D. Zhang, J. Pounders, A.M. Ougouag, "Simplified two and three dimensional HTTR benchmark problems," *Annals of Nuclear Energy*, Vol. 38, pp 1172-1185, 2011.
2. J.M. Pounders and F. Rahnema, "A response-based time-dependent neutron transport method," *Annals of Nuclear Energy*, Vol. 37, pp 1595-1600, 2010.
3. J.M. Pounders and F. Rahnema, "A Coarse-Mesh Method for the Time-Dependent Transport Equation," *Nuclear Science and Engineering*, 2013(accepted).
4. K.J. Connolly, F. Rahnema and D. Zhang, "A coarse mesh radiation transport method for 2-D hexagonal geometry," *Annals of Nuclear Energy*, Vol. 42, pp. 1-10, 2012.
5. K.J. Connolly and F. Rahnema, "A heterogeneous coarse mesh radiation transport method for neutronic analysis of prismatic reactors," *Annals of Nuclear Energy*, Vol. 56, pp 87-101, 2013.

### Conference papers:

6. A. Huning and S. Garimella, "Thermal Hydraulic Method for Whole Core Design Analysis of an HTGR," *International Conference on Mathematics and Computational Methods Applied to Nuclear Science and Engineering (M&C 2013)*, Sun Valley, Idaho, USA, May 5-9, 2013.
7. A. Huning and S. Garimella, "Full Core VHTR Steady State Thermal Hydraulic Simulation," *American Nuclear Society Annual Winter Meeting, Transactions of the American Nuclear Society*, Vol. 105, pp. 1038-39, Washington, D.C., October 30–November 3, 2011.
8. K. J. Connolly, A. J. Huning, F. Rahnema and S. Garimella, "Coupled Neutron Transport and Thermal Fluids Calculations for the VHTR," *Joint International Conference on Supercomputing in Nuclear Applications and Monte Carlo 2013 (SNA + MC 2013)*, La Cité des Sciences et de l'Industrie, Paris, France, October 27-31, 2013.
9. J. Pounders and F. Rahnema, "An integral response-based concept for solving the time-dependent transport equation," *2011 ANS Annual Meeting*; Hollywood, FL; United States; June 26-30, 2011.
10. K.J. Connolly and F. Rahnema, "Response expansion of incident angular flux and current for transport calculations," *2012 ANS Annual Winter Meeting*; San Diego, CA; United States; 11-15 November 2012.

11. K.J. Connolly, F. Rahnema and D. Zhang, "COMET-hex solution to a 2-D stylized high temperature test reactor benchmark," 2011 ANS Annual Meeting; Hollywood, FL; United States; June 26-30, 2011.
12. K.J. Connolly and F. Rahnema, "The comet method in 3-D hexagonal geometry," International Conference on the Physics of Reactors 2012: Advances in Reactor Physics, PHYSOR 2012; Knoxville, TN; United States; 15-20 April 2012.
13. D. Zhang and F. Rahnema, "Efficiency and accuracy of the perturbation response coefficient generation method for whole core comet calculations in BWR and CANDU configurations," International Conference on Mathematics and Computational Methods Applied to Nuclear Science and Engineering, M and C 2013; Sun Valley, ID; United States; 5-9 May 2013.
14. K. J. Connolly and F. Rahnema, and D. Zhang, "Efficiency and accuracy of the perturbation response coefficient generation method for whole core comet calculations in BWR and CANDU configurations," International Conference on Mathematics and Computational Methods Applied to Nuclear Science and Engineering, M and C 2013; Sun Valley, ID; United States; 5-9 May 2013.

### III. PROJECT TASKS

#### Task 1. Development of the response function (RF) generator in 2-D hexagonal geometry

##### 1. Task Status and Significant Results

###### a. Task Summary

Some background on this response expansion method is given in this section. The angular current on face  $f$  of mesh  $i$  can be expanded as

$$J_{if}^{\pm}(\vec{r}, \hat{\Omega}, E) = \sum_{a=1}^{\infty} c_{if}^a \Gamma^a(\vec{r}, \hat{\Omega}, E). \quad (1.1)$$

A method to generate the response expansion coefficients  $c_{if}^a$  from Eq. (1) is as follows. An incoming unit angular current distribution over one mesh face  $f$  is given as a source for a single mesh. Vacuum boundary conditions are specified, and no current enters from the other five faces, such that for the sake of Eq. (1.2),  $f' \neq f$ :

$$\begin{aligned} J_{if}^{-} &= \Gamma^a(\vec{r}, \hat{\Omega}, E) \\ J_{if'}^{-} &= 0 \end{aligned} \quad (1.2)$$

A separate fixed source calculation is conducted for an incoming current source on each phase space expansion order on each unique face of each unique mesh in the core. From each fixed-source calculation, the outgoing angular current  $J^+$  is determined for all six faces  $f'$ . Using the orthogonality relationship, we solve Eq. (1.1) for  $c_{if'}^{a'}$  given the calculated current exiting face  $f'$ :

$$c_{if'}^{a'} = \iiint J_{if'}^+(\vec{r}, \hat{\Omega}, E) \Gamma^{a'}(\vec{r}, \hat{\Omega}, E) d\vec{r} d\hat{\Omega} dE \quad (1.3)$$

For a complete set of coefficients, Eq. (1.3) must be solved for all expansion orders  $a'$ . Following in the method of Forget and Rahnema, a tensor product of shifted Legendre polynomials is chosen as the orthogonal set in which to expand the angular current:

$$\Gamma^a(\vec{r}, \hat{\Omega}, E) = \tilde{P}_l^{[0,U]}(u) \tilde{P}_m^{[-1,1]}(\mu) \tilde{P}_n^{[0,\pi]}(\varphi) \delta_g. \quad (1.4)$$

The reference system will be defined by the mesh face, where the spatial variable  $u$  extends along the length of the mesh face from 0 to  $U$ , the azimuthal angle  $\varphi$  from the mesh face is defined from 0 to  $\pi$ , and  $\mu$ , the cosine of the polar angle  $\theta$  from the mesh face, extends from -1 to 1. A more detailed description of the coordinate system used is presented with figures 1.1 and 1.2. The multigroup treatment of the energy variable over  $G$  groups is used. Therefore, the expansion coefficients for the angular current  $J^+$  exiting face  $f'$  of mesh  $i$ , in group  $g'$ , with spatial and angular expansion orders  $l'$ ,  $m'$ , and  $n'$  as a response to an incoming current on face  $f$  in group  $g$  having spatial and angular expansion orders  $l$ ,  $m$ , and  $n$  are defined as Eq. (1.5):

$$c_{i,f',g',l',m',n'}^{ifglmn} = \iiint J_{if'}^+(u, \mu, \varphi, E) \tilde{P}_l^{[0,U]}(u) \tilde{P}_m^{[-1,1]}(\mu) \tilde{P}_n^{[0,\pi]}(\varphi) \delta_g du d\mu d\varphi. \quad (1.5)$$

Since in a hexagonal mesh, the spatial and angular variables defined by each mesh face will have different orientations, and since the planes defined by the mesh faces themselves are not linearly independent, it is evident that a set of coordinate transformations must be introduced. The Cartesian coordinate system is used here for the sake of simplicity. Fig. 1.1 depicts a typical hexagonal mesh in the Cartesian  $x$ - $y$  plane.

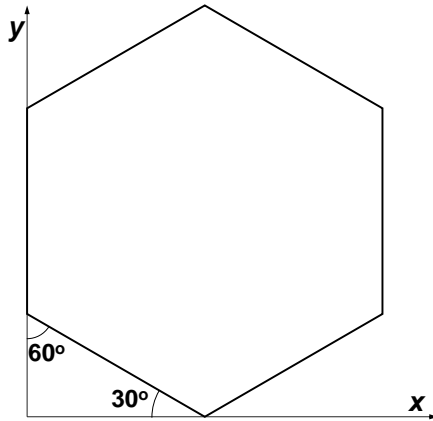
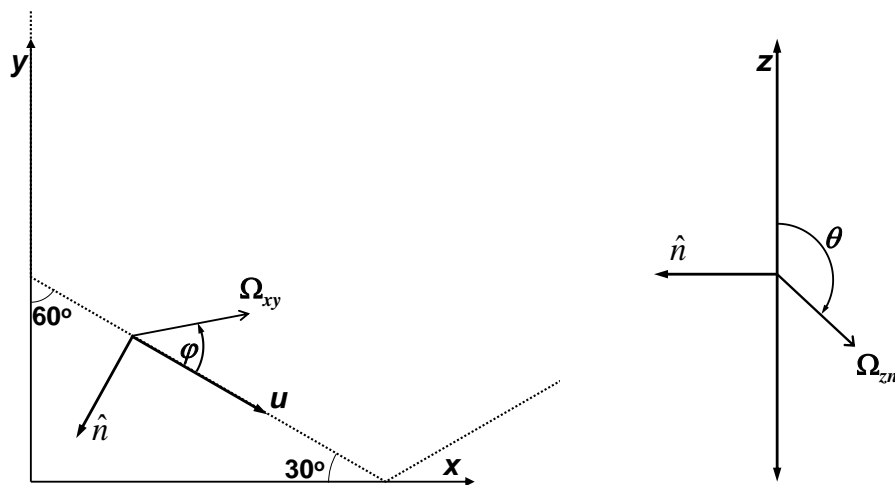


Fig. 1.1. Mesh geometry in Cartesian coordinates

To illustrate the concept of a different coordinate system for each mesh face, consider Fig. 1.2. An example incoming source particle will be traveling from some position  $u$  in direction  $\hat{\Omega}$  in three-dimensional space. Fig. 1.2a shows a portion of the mesh from Fig. 1.1, but is focused specifically on the lower-left mesh face; the mesh boundary is represented by a dashed line. The projection of the direction vector  $\hat{\Omega}$  onto the  $x$ - $y$  plane is shown along with the angle  $\varphi$ , and the relation of the spatial coordinate  $u$  for this particular mesh face to the Cartesian  $x$ - $y$  plane can be seen. The outward normal unit vector  $\hat{n}$  from the mesh face is also shown. Fig. 1.2b projects the direction vector onto the plane defined by the Cartesian  $z$  axis and the outward normal of the mesh face  $\hat{n}$ . The angle  $\theta$  is displayed, from which  $\mu$  can be calculated.



(a) projection onto  $x$ - $y$  plane

(b) projection onto  $z$ - $n$  plane

Fig. 1.2. Mesh coordinate systems for incoming source particles

The spatial coordinate  $u$ , defined along each mesh face, must be transformed into a coordinate in the Cartesian  $x$ - $y$  plane. Similarly, the angles  $\varphi$  and  $\mu$  defined from each mesh face must be transformed into some combination of the angular components  $\Omega_x$ ,  $\Omega_y$ , and  $\Omega_z$ . As an example, the Cartesian angular components for the illustrated face are found using Eq. (1.6):

$$\begin{aligned}\Omega_x &= \sqrt{1-\mu^2} \cos\left(\varphi - \frac{\pi}{6}\right) \\ \Omega_y &= \sqrt{1-\mu^2} \sin\left(\varphi - \frac{\pi}{6}\right) \\ \Omega_z &= \mu\end{aligned}\tag{1.6}$$

A similar set of equations may be determined for each mesh face. In this way, the incoming angular current surface source defined by Eq. (1.2) is applied to the coarse mesh.

Neutrons will be transported through the mesh, with some being eventually absorbed within the mesh, and the rest escaping. An exiting neutron will be at some position along a mesh face and traveling in some direction defined in Cartesian geometry. A second coordinate transformation must be applied in order to solve Eq. (1.5), placing Cartesian coordinates back into the  $u$ ,  $\varphi$ , and  $\mu$  phase space variables defined by the mesh face. However, the coordinate system for particles leaving the mesh must be oriented so that the angular half-space over which the orthogonal expansion of the angular current is defined is that space outside of the mesh. This must be done so that the current exiting one mesh is the same as that entering the adjacent mesh. Fig. 1.3 shows an example mesh and its neighboring meshes; the mesh face coordinate systems for incoming neutrons are shown as dashed lines inside of the hexagonal meshes, while the mesh face coordinate systems for neutrons exiting the meshes are given as solid lines outside of the hexagonal meshes. The coordinate system used for particles exiting each mesh face is the same as the coordinate scheme for particles entering the neighboring mesh face.

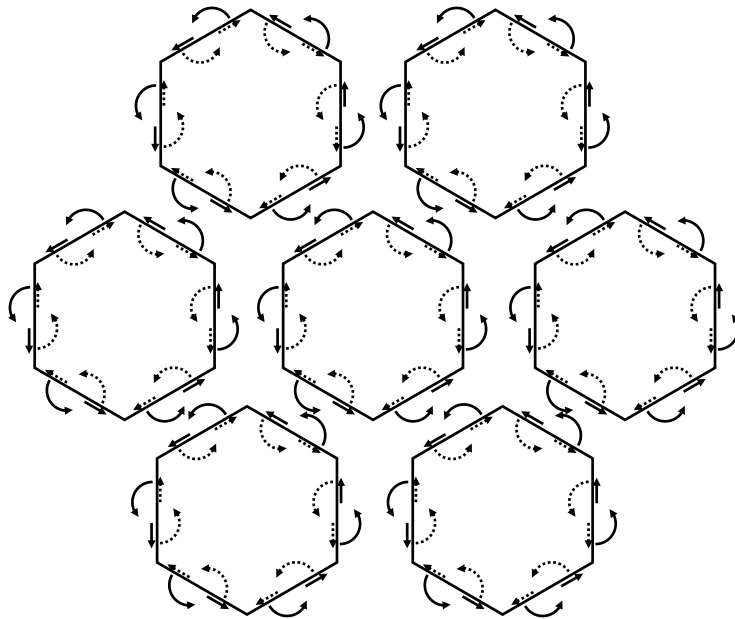


Fig. 1.3. Interactions between meshes

b. Task Status/Progress

The two dimensional hexagonal method was tested using a variety of benchmark core configurations based on the HTTR core described in the section on Task 3: Development of a set of 2-D hexagonal benchmark problems. A sampling of results is presented in Table 1.1, where the COMET results for a partially controlled core are compared with the MCNP benchmark solution. The figures presented in the tables represent the relative differences between COMET and MCNP in eigenvalue, block-averaged fission density, and pin fission density, along with the uncertainty figures associated with the eigenvalue and fission density calculations as determined by COMET. The final entry on the table is the computation time required for COMET to compose the solution on a single processor in seconds. This compares quite favorably to the hours or days required on a computing cluster for an MCNP solution of comparable precision in pin fission reaction rates.

Table 1.1. Partially Controlled Core Expansion Order Analysis

	(2,2,2)	(4,2,2)	(2,4,4)	(4,4,4)
RE k-eff (pcm)	27	41	-26	-10
$\sigma_{k\text{-eff}}$ (pcm)	2	2	2	2
Block AVG %	0.040	0.022	0.023	0.008
Block RMS %	0.043	0.024	0.027	0.010
Block MRE %	0.039	0.022	0.023	0.008
Block MAX %	0.069	0.044	0.046	0.022
Pin AVG %	0.079	0.045	0.067	0.032
Pin RMS %	0.128	0.057	0.118	0.039
Pin MRE %	0.069	0.043	0.057	0.031
Pin MAX %	0.791	0.222	0.732	0.123
AVG $\sigma_{\text{pin}}$ (%)	0.020	0.020	0.020	0.020
MAX $\sigma_{\text{pin}}$ (%)	0.025	0.025	0.026	0.026
Time (s)	63	172	178	482

**Task 2. Development of the deterministic sweeping method in 2-D hexagonal geometry**

1. Task Status and Significant Results

a. Task Summary

The final step in the method is a deterministic sweep which composes the solution to the problem. Each mesh within the core is solved in sequence to determine the angular current response expansion coefficient at each face. Since the solutions of the fixed-source transport problems within each mesh are independent of the solutions in neighboring meshes, the choice of sweeping order should not affect the accuracy of the solution. However, differing sweeping techniques influence the speed of the convergence of the solution. A diagram of three sweeping methods is included in Fig. 2.1.

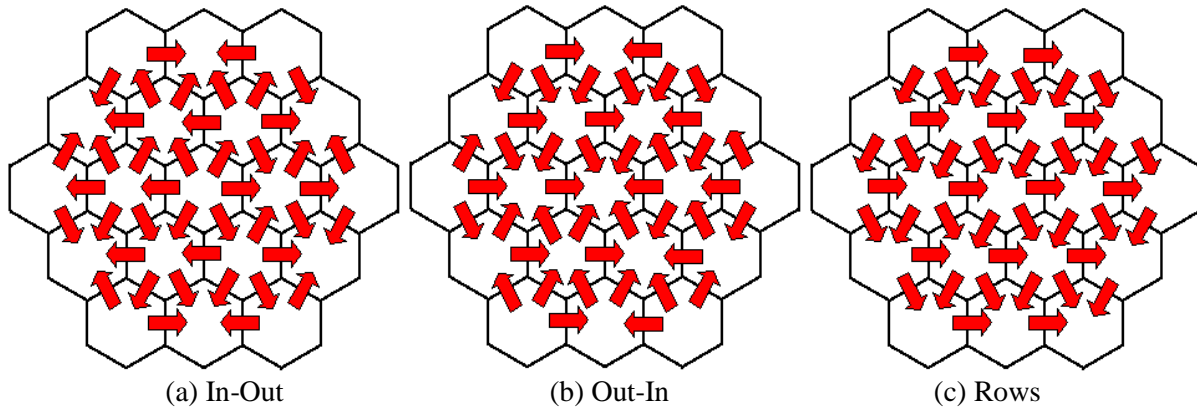


Fig. 2.1. Mesh sweeping schemes

#### b. Task Status/Progress

An outward and an inward sweeping scheme, both of which sweep symmetrically through the core, have been tested. It was determined that there was no difference in accuracy between the two sweeping orders, although the scheme depicted in Fig. 2.1a did lead to faster convergence of the solution. Forget et al. recommended that the sweeping order be chosen based on the symmetry of the problem; indeed, the asymmetric sweeping method depicted in Fig. 2.1c was found to be significantly less efficient in coming to a converged solution than the other two sweeping schemes.

### Task 3. Development of a set of 2-D benchmark problems

#### 1. Task Status and Significant Results

##### a. Task Summary

To assess the accuracy of diffusion or transport methods for reactor calculations, it is desirable to create heterogeneous benchmark problems that are typical of whole core configurations. We have created two and three dimensional numerical benchmark problems typical of high temperature gas cooled prismatic cores. Additionally, a single cell and single block benchmark problems are also included. These problems were derived from the HTTR start-up experiment. Since the primary utility of the benchmark problems is in code-to-code verification, minor details regarding geometry and material specification of the original experiment have been simplified while retaining the heterogeneity and the major physics properties of the core from a neutronics viewpoint. A six-group material (macroscopic) cross section library has been generated for the benchmark problems using the lattice depletion code HELIOS. Using this library, Monte Carlo solutions are presented for three configurations (all-rods-in, partially-controlled and all-rods-out) for both the 2D and 3D problems. These solutions include the core eigenvalues, the block (assembly) averaged fission densities, local peaking factors, the absorption densities in the burnable poison and control rods, and pin fission density distribution for selected blocks. Also included are the solutions for the single cell and single block problems.

##### b. Task Status/Progress

The benchmark specifications, problems, and their solution were published in *Annals of Nuclear Energy*. These problems have been used extensively in the development of the hexagonal neutronics method, and also by research groups elsewhere to benchmark their own transport methods under development.

## Task 4. Development of the 1-D time dependent RF generation method

### 1. Task Status and Significant Results

#### a. Task Summary

To limit the attention and scope of this work to the time dependence of the transport problem, the spatial domain will be restricted to one dimension. This restriction additionally limits the domain of neutron directions to one dimension (in the polar angle). For notation, we therefore define the phase space (i.e. the space-angle domain) as

$$\mathfrak{R} = V \times \Omega$$

with  $V = [a, b]$  and  $\Omega = [-1, 1]$ . The time domain will be defined, without loss of generality, as the positive real line:

$$\mathfrak{T} = [0, \infty)$$

The boundary of the phase space will be decomposed into four elements corresponding to the positive and negative angular half-spaces ( $\Omega^-$  and  $\Omega^+$ , respectively) at the two boundary points:

$$\partial\mathfrak{R}_a^\pm = \{a\} \times \Omega^\pm$$

$$\partial\mathfrak{R}_b^\pm = \{b\} \times \Omega^\pm$$

In this simplified context, the time-dependent transport equation can be written as

$$\frac{1}{v_g} \frac{\partial \psi_g(x, t)}{\partial t} + \mathbf{H}_g \psi_g(x, t) = q_g(x, t), \quad g = 1, 2, \dots, G \quad (4.1)$$

with  $(x, t) \in \mathfrak{R} \times \mathfrak{T}$  and the operator  $\mathbf{H}_g$  defined by

$$\begin{aligned} \mathbf{H}_g \psi_g(x, t) = & \mu \frac{\partial \psi_g(z, \mu, t)}{\partial z} + \sigma_g(z, t) \psi_g(z, \mu, t) \\ & - \sum_{g'=1}^G \sigma_{\text{eff}, g'}(z, t) \int_{-1}^1 f_{g', g}(z, \mu \mu', t) \psi_{g'}(z, \mu', t) d\mu', \end{aligned}$$

Because the current work is principally focused on the time dependence of the transport problem, the multigroup subscripts will be omitted; the quantity  $\psi(x, t)$  will therefore denote a scalar-valued function in one-group contexts and a vector-valued function otherwise. To complete the problem definition boundary and initial conditions must be specified. Time-dependent boundary conditions are prescribed in terms of arbitrary boundary operators:

$$\begin{aligned} j^-(x_a^-, t) &= \mathbf{B}_a j^+(x_a^+, t), \quad x_a^\pm \in \partial\mathfrak{R}_a^\pm \\ j^-(x_b^-, t) &= \mathbf{B}_b j^+(x_b^+, t), \quad x_b^\pm \in \partial\mathfrak{R}_b^\pm \end{aligned} \quad (4.2)$$

with the partial currents defined with respect to the surface outward normal directions as

$$\begin{aligned}
j^+(x,t) &= n(x)\mu\psi_g(x,t), \\
j^-(x,t) &= n(x)\mu\psi_g(x,t), \\
n(x) &= \begin{cases} +1, & x \in \partial\mathfrak{R}_a^- \cup \partial\mathfrak{R}_b^+ \\ -1, & x \in \partial\mathfrak{R}_a^+ \cup \partial\mathfrak{R}_b^- \\ 0, & \text{otherwise} \end{cases}
\end{aligned}$$

Additionally, a given initial condition is prescribed on the angular flux at time  $t=0$ :

$$\psi(x,0) = \psi^0(x), \quad x \in \mathfrak{R} \quad (1)$$

Equation (4.1) along with conditions **Error! Reference source not found.** and (1) constitute the *global problem*, in contrast to the *local problem* that will be discussed in the following subsection.

The primary philosophical approach of the coarse-mesh transport (COMET) method can be summarized in two steps:

1. decompose the global problem into a series of local problems; then
2. couple the local problems using response functions to reconstruct the global problem solution.

The decomposition of the global problem into a sequence of local problems is discussed next, followed by a construction of the response-based framework for the global-local coupling. Both of these sections follow the principles utilized in the previous steady-state COMET work, but are rigorously repeated and extended here with the inclusion of the time variable.

### Global-Local Decomposition

To decompose the global problem into a sequence of local problems, the system volume,  $V$ , is partitioned into  $N$  non-overlapping sub-regions (coarse meshes). Specifically, if the mesh is

defined by the set of points  $\{z_n\}_{n=0}^N$  such that  $z_0 = a$ ,  $z_N = b$  and  $z_{n-1} < z_n$  for  $1 \leq n \leq N$ , then the local problem phase spaces can be defined by

$$\begin{aligned}
\mathfrak{R}_n &= [z_{n-1}, z_n] \times \Omega, \quad 1 \leq n \leq N \\
\partial\mathfrak{R}_n^\pm &= \{z_n\} \times \Omega^\pm, \quad 0 \leq n \leq N
\end{aligned}$$

The local problem is now formed by restricting Equation

**Error! Reference source not found.** to one of the  $\mathfrak{R}_n$  sub-spaces:

$$v^{-1} \frac{\partial \psi_n(x,t)}{\partial t} + \mathbf{H} \psi_n(x,t) = q_n(x,t), \quad (x,t) \in \mathfrak{R}_n \times T, \quad (4.4)$$

where the  $n$  subscripts have been added to note the problems local domain. The local problem boundary conditions are formed by replacing the external (partial current) boundary condition operators of Equation (4.2) with the incoming partial currents from adjacent mesh cells:

$$\begin{aligned}
j_n^-(x_{n-1}, t) &= j_{n-1}^+(x_{n-1}, t), \quad x_{n-1} \in \partial\mathfrak{R}_{n-1}^+ \\
j_n^-(x_n, t) &= j_{n+1}^+(x_n, t), \quad x_n \in \partial\mathfrak{R}_n^-
\end{aligned} \quad (4.5)$$

The initial condition is formed by simply restricting  $\psi_0(x)$  to  $\mathfrak{R}_n$ :

$$\psi_n(x,0) = \psi_n^0(x), \quad x \in \mathfrak{R}_n \quad (4.6)$$

Equations (4.4-6) now constitute  $N$  local problems derived from the global problem given in the previous section.

At this point, no approximations have been in decomposing the global problem: the collection of the local problem solutions,  $\psi_n(x, t)$ , are together equivalent to the global problem solution. This formulation is useful because it facilitates a decoupling of the local problems. Specifically, it can be seen that each local problem is completely independent of all others except for the time-dependent flow of neutrons through its bounding surfaces. In Section 2.4, the boundary sources will be approximated in a way that permits a complete decoupling of the local problems. First, however, a generalized response equation is derived to compactly and explicitly represent the local problem solutions in terms of the local boundary and initial conditions.

### The Response Equation

As the name implies, a response equation describes the neutronic response of a system given some source term. The driving sources in Equation (4.4) are the initial condition [Equation (4.6)] and boundary sources [Equation (4.5)]. Rather than applying these sources as conditions on the transport equation, it will be useful in the subsequent analysis to include them as explicit source terms, so that Equation (4.1) has the form

$$v^{-1} \frac{\partial \psi_n(x, t)}{\partial t} + \mathbf{H} \psi_n(x, t) = q_n(x, t) + q_n^{BC}(x, t) + q_n^{IC}(x) \delta(t) \quad (4.7)$$

where the two additional terms represent the boundary and initial conditions, respectively, and  $\delta(t)$  is the Dirac delta function. Note that because the boundary and initial *sources* are included explicitly in this expression, the boundary and initial *conditions* are replaced by free-surface and zero initial conditions, respectively.

The incoming partial currents in Equation (4.5) already have the correct definition as a source terms, so the boundary source may be simply defined as

$$q_n^{BC}(x, t) = \chi_{\partial \mathfrak{R}_{n-1}^+}(x) j_{n-1}^+(x_{n-1}, t) + \chi_{\partial \mathfrak{R}_n^-}(x) j_{n+1}^+(x_n, t) \quad (4.8)$$

where  $\chi_{\partial \mathfrak{R}_a^\pm}$  is the characteristic function, satisfying

$$\chi_{\partial \mathfrak{R}_{a/b}^\pm}(x) = \begin{cases} 1, & x \in \partial \mathfrak{R}_{a/b}^\pm \\ 0, & x \notin \partial \mathfrak{R}_{a/b}^\pm \end{cases}$$

A similar expression for the initial source can be derived by integrating Equation **Error! Reference source not found.** over an infinitesimal time interval centered at time  $t = 0$ :

$$v^{-1} \lim_{\delta \rightarrow 0} [\psi_n(x, +\delta) - \psi_n(x, -\delta)] = q_n^{IC}(x) + \lim_{\delta \rightarrow 0} \int_{-\delta}^{+\delta} [-\mathbf{H} \psi_n(x, t) + q_n(x, t) + q_n^{BC}(x, t)] dt \quad (4.9)$$

The fact that there are no sources defined for  $t < 0$  implies that  $\lim_{t \rightarrow 0^-} \psi(x, t) = 0$ . Therefore, Equation (4.9) reduces in the right-hand limit to

$$v^{-1} \psi_n(x, t) = q_n^{IC}(x) \quad (4.10)$$

Requiring that the original initial condition, Equation (1), hold provides a definition for the initial source term:

$$q_n^{IC}(x) = v^{-1} \psi_n^0(x) \quad (4.11)$$

Inserting this definition along with the boundary source term into Equation (4.7) results in

$$v^{-1} \frac{\partial \psi_n(x, t)}{\partial t} + \mathbf{H} \psi_n(x, t) = q_n(x, t) + \chi_{\partial \mathbb{R}_{n-1}^+}(x) j_{n-1}^+(x_{n-1}, t) + \chi_{\partial \mathbb{R}_n^-}(x) j_{n+1}^+(x_n, t) + v^{-1} \psi_n^0(x) \delta(t) \quad n = 1, 2, \dots, N \quad (4.12)$$

Equation (4.12) accounts for all neutron sources explicitly, rather than using initial and boundary conditions. Because the solution of the transport equation is linear in its source terms, one could write the flux as a linear combination of four components with respect to the four source terms on the right-hand-side of Equation (4.12). If each of these components is expressed as a generalized response to a given source, then it follows that the angular flux may be written in

$$\begin{aligned} \psi_n(x, t) = & R[x, t, q_n] + \\ & + R[x, t, j_{n-1}^+] + \\ & + R[x, t, j_{n+1}^+] + \\ & + R[x, t, v^{-1} \psi_n^0] \end{aligned} \quad (4.13)$$

where  $R$  is a functional that, given some space- and time-dependent source, returns the flux response at point  $(x, t)$ . This functional can in fact be defined specifically in terms of the point-source Green's function associated with Equation (4.12):

$$R[x, t, \square] = \int_0^t dt' \int_{\mathbb{R}_n} dx' [\square] G_n(x' \rightarrow x, t' \rightarrow t) \quad (4.14)$$

where the Green's function satisfies

$$\frac{1}{v} \frac{\partial G_n(x' \rightarrow x, t' \rightarrow t)}{\partial t} + \mathbf{H} G_n(x' \rightarrow x, t' \rightarrow t) = \delta(x - x') \delta(t - t')$$

A similar equation for the surface partial currents can be obtained by simply multiplying both sides of Equation (4.13) by  $|\mu|$  and evaluating at the boundary points.

Equation (4.13) is an ideal form of the response equation: it provides a formula for the angular neutron flux (and surface partial currents) in terms of arbitrary neutron sources and a response kernel (the Green's function). Ultimately it will be shown that the response equation for the angular flux [Equation(4.13)] is primarily useful for coupling local transport solutions in *time*, while the corresponding equation for the partial currents is primarily useful for coupling local transport solutions in *space*. Also, in the next section it will be shown that there is no need to explicitly compute the Green's functions—they are presently used as a placeholder for an underlying (local) transport calculation. Nevertheless these response equations form the theoretical basis of the COMET method, and additional examples of the method's derivation are included in the reference (Pounders and Rahnema: A Coarse-Mesh Method for the Time-Dependent Transport Equation).

#### b. Task Status/Progress

The time dependent response expansion method was implemented into a computational framework as part of Task 5, described below.

### Task 5. Development of the 1-D time dependent sweeping method

## 1. Task Status and Significant Results

### a. Task Summary

To summarize the developments of the previous section, the solution of the time-dependent coarse-mesh transport can be obtained from a set of response equations over a coarse partition of the reactor phase space in a finite time interval. Approximate solutions of the response equations are obtained by projections onto polynomial spaces spanned by combinations of shifted Legendre polynomials. This formulation permits a convenient decoupling of the global problem into a sequence of local (coarse-mesh) transport problems that are characterized by response functions that can be calculated independently of the other local problems. As a result, the computational process can be divided into two phases:

1. Pre-computation: calculation of the response function coefficients for each coarse mesh;
2. Solution construction: coupling of the coarse meshes in space, angle and time by a deterministic algorithm.

This divided approach is very well suited for reactor problems because reactors are often modeled using only a finite number of unique fuel assemblies or blocks. Choosing a single fuel assembly as a coarse-mesh therefore means that one is able to reconstruct a full-core solution using only a relatively small number of response functions. The efficiency of this approach has been demonstrated in the steady-state work on this topic.

### b. Task Status/Progress

A semi-infinite medium ( $z \in [0, \infty]$ ) with an oscillating impinging current,

$\Gamma_0(t) = 1 + \sin \omega t$ , is studied in this example. Because this is an infinite-medium fixed-source problem, there is no volumetric initial source, and the only response that needs to be calculated is the exiting partial currents. The response equations therefore simplify to

$$j^+(x_0, t) = \int_0^t dt' \int_{\partial\mathbb{R}^+} dx' \Gamma_0(x', t') \bar{G}_n^{g' \rightarrow g}(x' \rightarrow x_0, t' \rightarrow t),$$

which has the following approximate form:

$$\mathbf{j}^{(q)+}(z_0) = \sum_{q'=0}^Q \bar{\mathbf{R}}_q^q \Gamma_0^{(q')}(z_0)$$

The time-expansion coefficients of the incident source were calculated using the adaptive-recursive Simpson's rule in MatLab<sup>®</sup>. This example primarily serves to test the approximation of the surface-to-surface time-convolution approximation.

Figure 5.1 shows the solution using an 11<sup>th</sup> order time-expansion and a histogram plot of the MCNP Monte Carlo reference solution. Table 5.1 presents the average (AVG), root-mean-square (RMS) and maximum (MAX) errors of the solution integrated over each of the MCNP time bins.

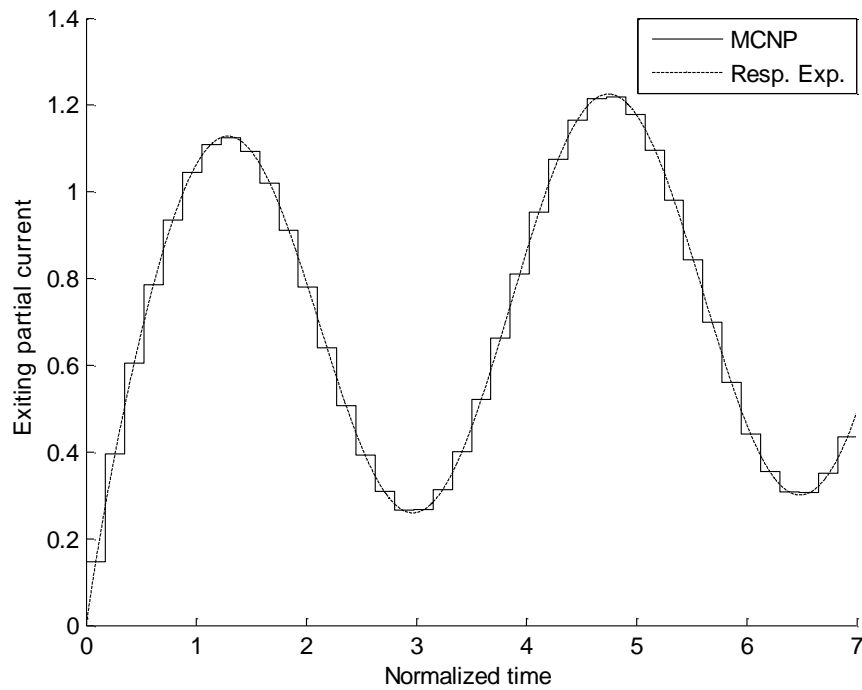


Figure 5.1: Example 3, plot of 11<sup>th</sup> order response solution and MCNP reference solution histogram

Table 5.1: Example: Bin-Integrated Error Statistics

Expansion order	AVG	RMS	MAX
8	2.76%	3.60%	8.34%
11	0.14%	0.18%	0.41%
14	0.02%	0.03%	0.08%
17	0.02%	0.03%	0.09%

Additional examples of the method’s performance are included in the reference (Pounders and Rahnema: A Coarse-Mesh Method for the Time-Dependent Transport Equation).

## Task 6. 1-D time dependent benchmark problems

Four example problems are used to test the 1-D time-dependent COMET. These examples are roughly in order of increasing complexity.

### 6.1 Olson-Henderson Slab

The first problem that is considered is a homogeneous, finite slab. The slab initially has no neutrons, and at time  $t = 0$  a uniform, isotropic source is “turned on” and remains on for the duration of the problem, eventually evolving to a steady-state distribution. The slab is ten mean-free-paths in width with vacuum boundary conditions and is not fissionable; the ratio of the

scattering to the total cross section is 0.9. This problem was chosen because there is an analytical solution available in the literature (Olson and Henderson 2004).

Fig. 6.1 shows the analytical, COMET and discrete ordinates (S32) flux solutions as a function of space at 1.0, 2.5, 5.0, 7.5 and 10 mean-free-times. The COMET solution was generated using a 5th order angular expansion, 10th order spatial expansion and 10<sup>th</sup> order time expansion.

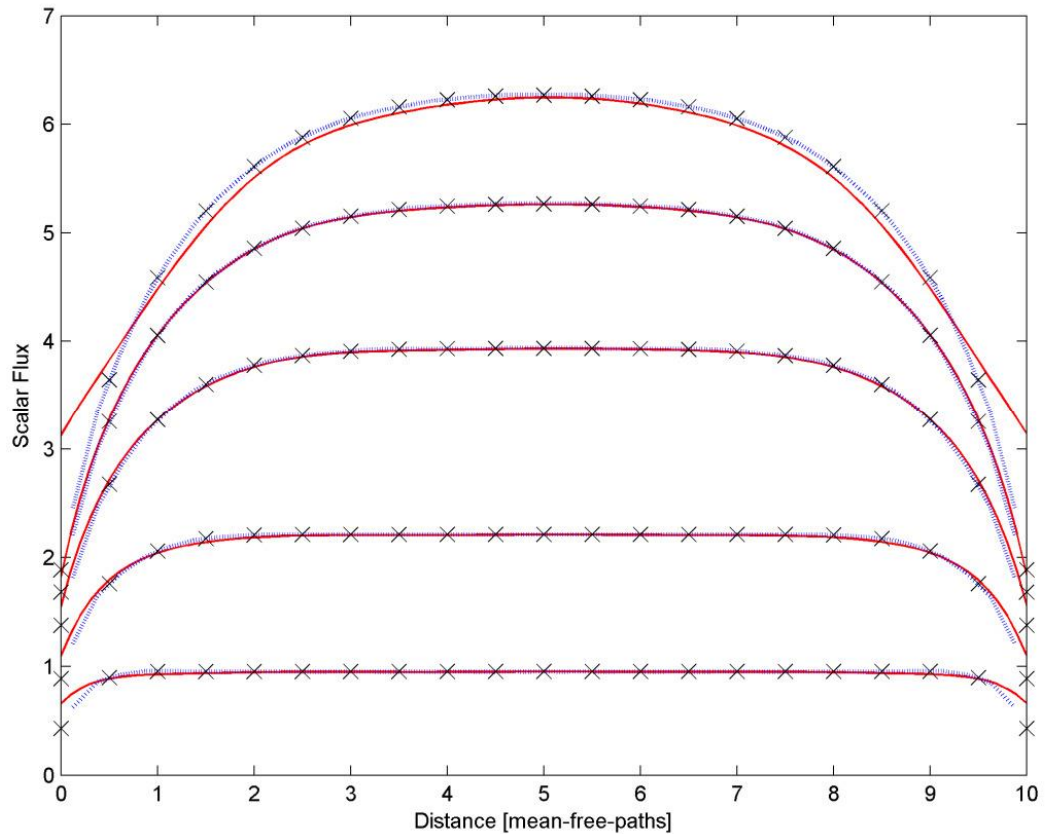


Fig. 6.1: Example 1, analytical (crosses), discrete ordinates (blue) and COMET (red) flux distributions; solutions shown at  $t = 1.0, 2.5, 5.0, 7.5, 10$  mean-free times

## 6.2 Infinite Medium Example

The second problem is infinite and homogeneous in the spatial dimension. Although the problem is physically an infinite medium, it is modeled in COMET as a finite slab with specular reflection boundary conditions to verify the theory and the implementation of the new time-dependent theory.

Fig. 6.2 shows the converged COMET solutions with time steps equal to 7 and 21 using a 15th order time expansion (the results are accurate enough that the plots are visually indistinguishable).

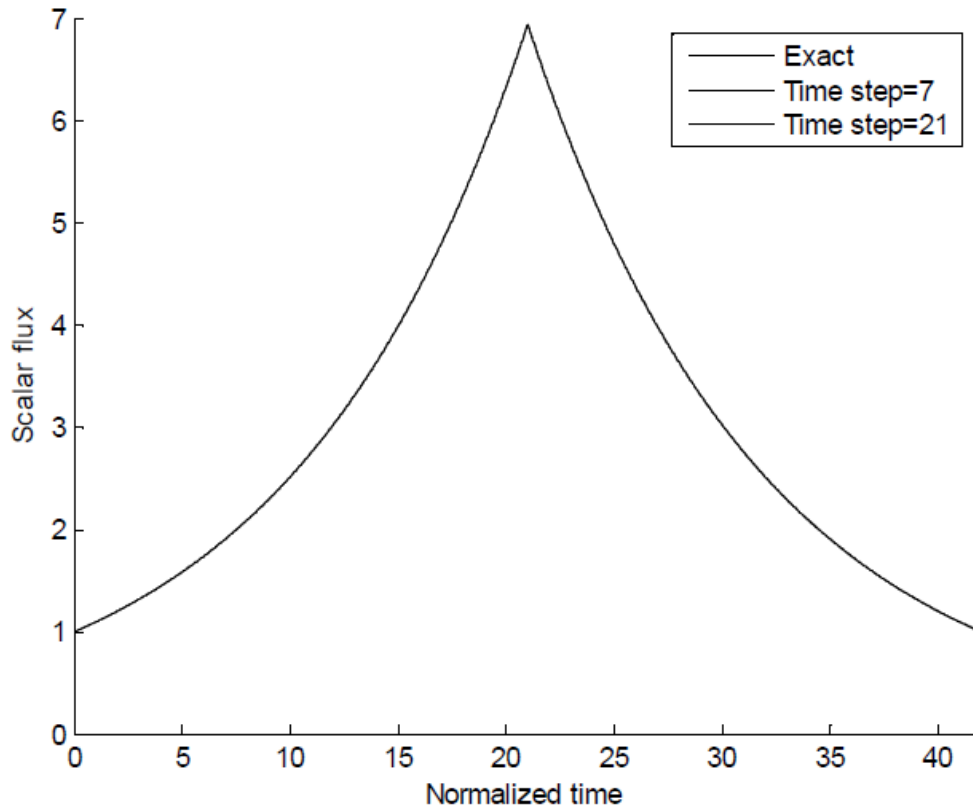


Fig. 6.2 Example 2, plot of scalar flux vs. time for exact solution and 15th order response-based solutions with time steps equal to 7 and 21

### 6.3 Semi-Infinite Medium With Time-Varying Incident Source

A semi-infinite medium ( $z \in [0, \infty]$ ) with an oscillating impinging current,  $\Gamma(t) = 1 + \sin \omega t$ , is studied in this example. Because this is an infinite-medium fixed source problem, there is no volumetric initial source, and the only response that needs to be calculated is the exiting partial currents. The solution to this problem is present in Task 5.

### 6.4 ANL Fast Reactor Benchmark

In this last example, a 2-group heterogeneous fast reactor benchmark based on Benchmark 16 from the Argonne National Laboratory Benchmark Problem Book (1985) is examined.

The reactor consists of seven homogeneous regions that are summarized in Table 6.1. The solutions presented here include prompt neutrons only. The initial critical flux distributions are shown in Figure 6.3. The discrete ordinates solution uses 32-point Gauss-Legendre quadrature in angle and a finite difference scheme spatially; the COMET solution uses an 8th order angular expansion and 15th order expansion in space. The comparison of the critical flux configuration is shown in Fig. 6.4

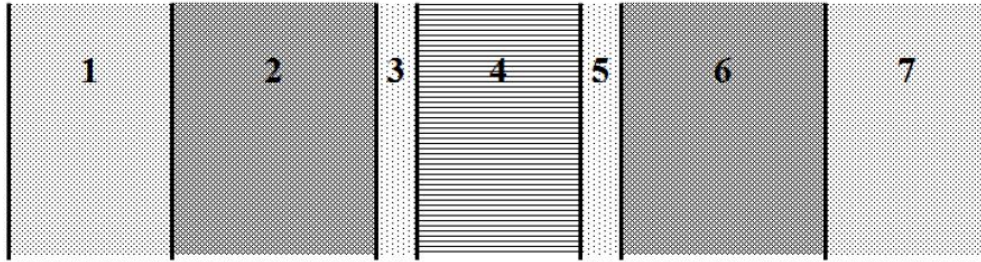


Fig. 6.3 ANL Benchmark Geometry

Table 6.1 ABL Benchmark Characteristics

Zone	Material	Width [cm]	$\nu\sigma_{f,1}/\sigma_1$	$\nu\sigma_{f,2}/\sigma_2$	$\sigma_{a,1}/\sigma_1$	$\sigma_{a,2}/\sigma_2$
1, 7	Blanket	40.000	3.461E-03	7.856E-04	1.600E-02	2.444E-02
2, 6	Outer Core	47.374	4.030E-02	3.016E-02	2.760E-02	3.566E-02
3, 5	Control Rod	9.000	0.000E+00	0.000E+00	7.308E-02	8.693E-02
6	Inner Core	34.000	4.030E-02	3.016E-02	2.760E-02	3.566E-02

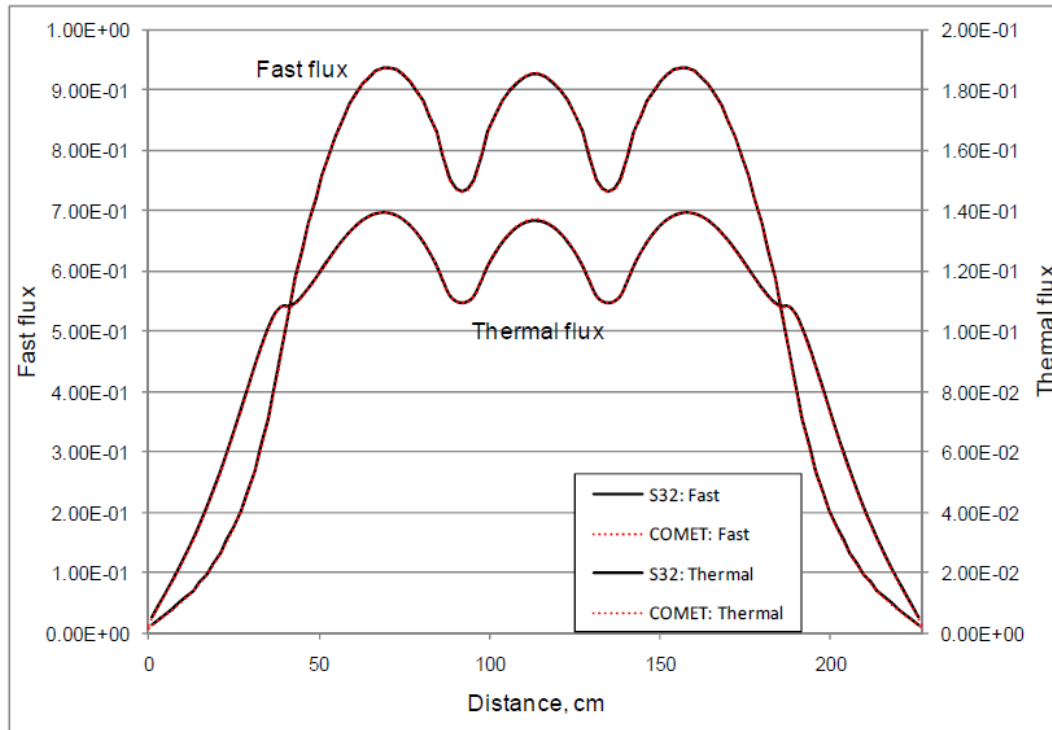


Fig. 6.4 ABL Benchmark Critical Flux Configuration

## Task 7. Development of a flux expansion method for 3-D hexagonal configurations

### 1. Task Status and Significant Results

#### a. Task Summary

For the 2-D method described in Task 1, the incident angular current was used as the boundary condition for coarse mesh fixed source problems. This treatment expanded the angular current as

$$\beta_{if}^{\pm}(\vec{r}, \hat{\Omega}, E) = J_{if}^{\pm}(\vec{r}, \hat{\Omega}, E). \quad (7.1)$$

The orthogonal set used in this case was the product of the shifted Legendre polynomials over position and angle, as given by Eq. (7.2):

$$\Gamma^a(\vec{r}, \hat{\Omega}, E) = \tilde{P}_l^{[0,U]}(u) \tilde{P}_m^{[0,V]}(v) \tilde{P}_n^{[-1,1]}(\mu) \tilde{P}_p^{[0,\pi]}(\varphi) \delta(E - E_g). \quad (7.2)$$

From this point onward, the position  $\vec{r}$  will be given in terms of the spatial variables  $u$ , which is defined along one direction of the mesh face from 0 to  $U$ , and  $v$ , which represents the position in the other dimension of the mesh face between 0 and  $V$ . The direction  $\hat{\Omega}$  will be given in terms of the cosine  $\mu$  of the polar angle  $\theta$  from the mesh face, and the azimuthal angle  $\varphi$ . The delta function is used to specify a multigroup (discrete) energy treatment over  $G$  groups.

The expansion coefficient for the angular current  $J^+$  exiting face  $f'$  of mesh  $i$ , in group  $g'$ , with spatial and angular expansion orders  $l'$ ,  $m'$ ,  $n'$ , and  $p'$ , as a response to an incoming current on face  $f$  in group  $g$  being of spatial and angular expansion orders  $l$ ,  $m$ ,  $n$ , and  $p$ , is determined as follows:

$$c_{i,f',g',l',m',n',p'}^{ifglmp} = \iiint \iiint J_{if}^+(u, v, \mu, \varphi, E) \tilde{P}_l^{[0,U]}(u) \tilde{P}_m^{[0,V]}(v) \tilde{P}_n^{[-1,1]}(\mu) \tilde{P}_p^{[0,\pi]}(\varphi) \delta(E - E_g) du dv d\mu d\varphi dE \quad (7.3)$$

However, coincident research in water-moderated reactors has suggested that expanding the incident angular flux in a combination of the Legendre polynomials over the spatial domain, the Legendre expansion of the cosine of the azimuthal angle, and the Chebyshev polynomial of the second kind defined over the cosine of the polar angle yields better results, as such an expansion preserves not only the particle balance at the mesh interfaces, but also describes an isotropic flux at the boundary when the 0<sup>th</sup> order is used. As the angular flux has a large isotropic component in highly scattering reactors, it has been suggested that expanding the angular flux requires a lower order of expansion to achieve similarly accurate results when compared to an angular current expansion at the mesh boundary. The use of angular flux as the physical quantity of expansion changes the boundary condition to

$$\beta_{if}^{\pm}(\vec{r}, \hat{\Omega}, E) = \psi_{if}^{\pm}(\vec{r}, \hat{\Omega}, E), \quad (7.4)$$

and the expansion function is defined

$$\Gamma^a(\vec{r}, \hat{\Omega}, E) = \tilde{P}_l^{[0,U]}(u) \tilde{P}_m^{[0,V]}(v) \mathcal{U}_n^{[-1,1]}(\mu) \tilde{P}_p^{[0,\pi]}(\cos \varphi) \delta(E - E_g). \quad (7.5)$$

The coefficients may be found

$$c_{i,f',g',l',m',n',p'}^{ifglmp} = \iiint \iiint \psi_{if}^+(u, v, \mu, \varphi, E) \tilde{P}_l^{[0,U]}(u) \tilde{P}_m^{[0,V]}(v) \mathcal{U}_n^{[-1,1]}(\mu) \tilde{P}_p^{[0,\pi]}(\cos \varphi) \delta(E - E_g) du dv d\mu d\varphi dE \quad (7.6)$$

An investigation of these boundary conditions using benchmarks based on the HTTR and on a smaller test core was conducted, and it was concluded that a response expansion of the angular flux presents the superior boundary condition to the current expansion used previously.

### *Treatment of Hexagonal Geometry*

Previously, the COMET method has been used in 2-D hexagonal geometry and in both 2-D and 3-D Cartesian geometry. In these cases, the faces of the coarse meshes are represented as either one dimensional line segments (in 2-D problems) or as two dimensional rectangular faces (in 3-D Cartesian geometry). A hexagonal prismatic mesh has six rectangular faces, for which the existing method of expansion in the spatial variables  $u$  and  $v$  is adapted without modification. However, the top and bottom hexagonal faces present a new challenge: a new scheme is necessary in order to describe the mesh faces in two spatial dimensions.

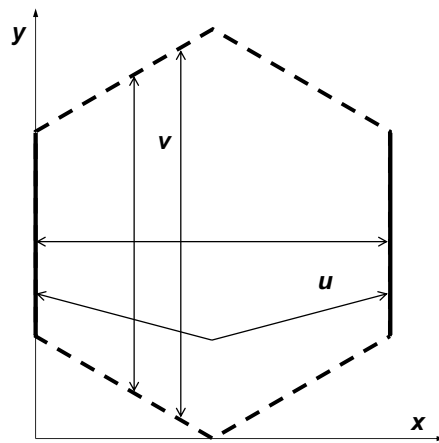


Figure 7.1. Top mesh face coordinates

The expansion over the two spatial variables is maintained over the hexagonal mesh faces. Figure 7.1 illustrates the top face of a hexagon, indicating the  $u$  and  $v$  axes over the mesh face. The  $u$  variable continues to indicate the position along the  $x$  axis, however, the  $v$  variable must be transformed from describing simply the  $y$  coordinate to describing the position in that direction with respect to the edges of the mesh face. This transformation means that the length from 0 to  $V$  in the  $v$  direction is no longer constant, but is a function of position in the  $u$  direction; when  $u$  is equal to 0.5,  $V$  represents a length which is double that when  $u$  is equal to 0 or 1.

#### b. Task Status/Progress

The theory for the flux expansion has been published and adapted into Task 8.

### **Task 8. Development of the RF generator for 3-D hexagonal geometry**

#### 1. Task Status and Significant Results

##### a. Task Summary

The response function generator was developed by implementing the theory as described in Task 7 into a modified version of MCNP5 and used in conjunction with the deterministic sweeping method described in Task 9.

b. Task Status/Progress

Results using the methods in Tasks 7 and 8, used with the method developed in Task 9, were successful; more detail is in the following section.

**Task 9. Development of the sweeping method for 3-D hexagonal geometry**

1. Task Status and Significant Results

a. Task Summary

The final step in the method is the deterministic iterative procedure which composes the solution to the whole core problem. Starting with an initial guess for the eigenvalue and flux distribution, the outgoing response to the hypothesized incoming current is determined for each mesh, proceeding in a given sweep order. It was previously shown (in Task 2) that the sweep order did not affect the accuracy of the solution, but that sweeping from the center of the core outward yielded results more efficiently than other sweeping methods which had been proposed. The method retains this outward sweeping scheme, in which new response expansion coefficients are first determined for the angular flux exiting the center mesh, based on an initial guess for the angular flux entering that mesh. The process repeats for each mesh in the core, with the sequence of meshes ordered in an outward sweep.

b. Task Status/Progress

Table 9.1 contains a comparison of results determined by the 3-D hexagonal COMET with those determined by a whole core Monte Carlo calculation. The first line is the expansion order of the calculation, where the numbers in parenthesis are the maximum orders of  $l$ ,  $m$ ,  $n$ , and  $p$  used in equation (7.6) for the synthesis of the solution. The following lines are the relative error/difference between COMET and MCNP in eigenvalue, followed by the uncertainty in the eigenvalue calculation. The next three lines are the errors in the pin fission density results: average absolute error, mean relative (flux weighted) error, and maximum absolute errors are presented. The computational runtime in minutes on a single processor is on the last line of the table, compared to hours or days on a large cluster for whole core Monte Carlo to solve the same problem. Results are given for a core configuration with some rods in, but many other core configurations were solved with similar accuracy. This is presented as a brief summary.

Table 9.1. SRI HTTR

	(2,2,2,2)	(2,2,4,4)	(4,4,2,2)	(4,4,4,4)
RE k (pcm)	56	45	22	21
$\sigma_k$ (pcm)	63	63	63	63
AVG %	0.34	0.37	0.34	0.34
MRE %	0.32	0.34	0.33	0.33
MAX %	1.98	1.90	1.28	1.28
runtime (min)	114	187	147	278

## **Task 10. Development of a set of 3-D benchmark problems**

### 1. Task Status and Significant Results

#### a. Task Summary

Alongside the 2-D benchmark problems developed in Task 3 using Japan's HTTR as a guide, several 3-D configurations were solved and published. A fully detailed description of all core configurations was given, along with material specifications and nuclear data in the form of multigroup cross sections.

#### b. Task Status/Progress

A set of 3-D hexagonal neutronics benchmarks accompanied the 2-D problems in Task 3.

## **Task 11. Development of a depletion module**

### 1. Task Status and Significant Results

In an operating nuclear reactor, the isotope composition of a nuclear fuel changes due to nuclides transforming to other nuclides via spontaneous radioactive decay and neutron-induced transmutation reactions. To take this effect into account, a fuel depletion capability is developed in this task to couple with the COMET neutronics module. One of the most widely used simulation methods is based on macro depletion techniques which calculate cross sections as a function of assembly averaged burnup as well as other core state parameters. These cross sections are generated by performing single assembly lattice depletion calculations. In this project, the whole-core depletion method in COMET is developed in a similar manner. The detailed description of numerical steps for COMET burnup calculations are presented below:

#### (1) Burnup rate dependent cross section generation

In the first step, HELIOS, which is an advanced lattice depletion code with both method of characteristics (MOC) and collision probability (CPM) solvers in general geometry, is used to generate multi-group cross sections for each region at a set of pre-defined burnup points,  $B_1, B_2, \dots, B_n$ .

#### (2) Response function library generation

The response function generator, a modified version of MCNP, is used to generate the response coefficient library for each unique assembly at the pre-defined burnup points.

#### (3) COMET whole core transport calculations

The response function library pre-computed in step (2) is used to perform whole core transport calculations. A detailed description can be found in tasks 2 and 9.

#### (4) Macro depletion calculation

The power distribution computed in step (3) is used to calculate the burnup rate in each region as:

$$\Delta B_i = \frac{\Delta B_c P_i / G_i}{P_c / G_c} \quad (11.1)$$

where  $\Delta B$ ,  $P$  and  $G$  represent the burnup increment, power and heavy metal loading, respectively, and subscripts “ $i$ ” and “ $c$ ” represent region  $i$  and the reactor core.

(5) Update response functions

Once the average burnup rate for each assembly is determined, the response function can be interpolated as:

$$R_i(B) = R_i(B_n) \frac{B_{n+1} - B}{B_{n+1} - B_n} + R_i(B_{n+1}) \frac{B - B_n}{B_{n+1} - B_n} \quad (11.2)$$

where  $R_i(B)$  is the response function for assembly  $i$  at burnup rate  $B$ .

The updated response functions are then used to perform new whole-core neutronics calculations at the new burnup rate.

To test the COMET depletion module, a 2D benchmark problem shown in Fig. 11.1 is used. The radial core geometry of the core consists of 4, 21.42 cm  $\times$  21.42 cm, fuel assemblies. Reflective boundary condition is assumed on the four external surfaces. Two types of fuel assembly (enriched and natural  $\text{UO}_2$ ) used in this problem are composed of 17x17 grid of pin cells as shown in Fig. 11.1. Each pin cell consists of a circular pin of fuel, and zirconium cladding and surrounding moderator. In enriched  $\text{UO}_2$  rods, the fuel is enriched to 3.68 wt% in U-235.

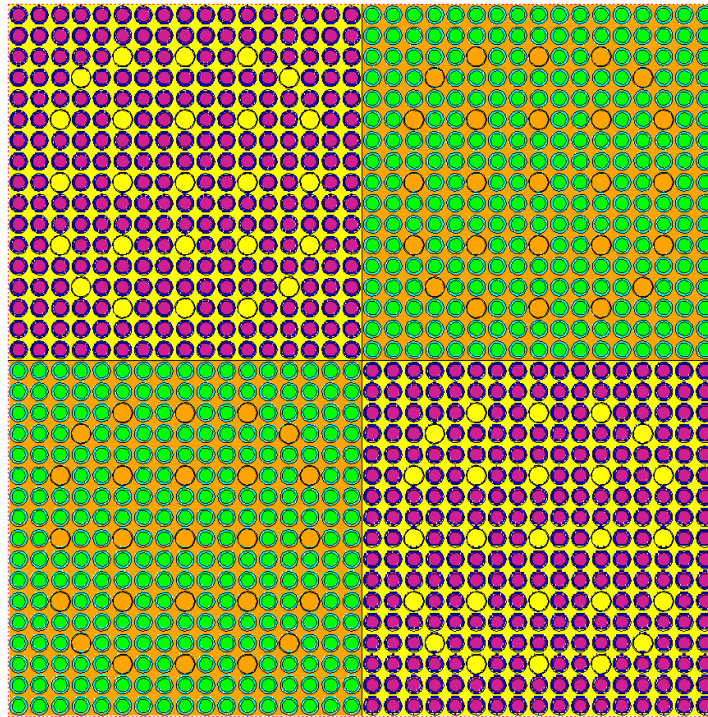


Fig. 11.1 2D 2X2 Benchmark problem

HELIOS is used to generate 2-group cross sections for the two assemblies at 35 different burnup rates: 0, 0.25, 0.5, 0.75, 1, 1.5, 2, 2.5, 3, 3.5, 4, 4.5, 5, 6, 7, 8, 9, 10, 12, 14, 16, 18, 20,

22, 24, 26, 28, 30, 32, 34, 36, 38, 40, 42, and 44 GWd/tU. The response function library based on these 2-group cross sections is used to perform COMET whole-core calculations for the benchmark problem described above. HELIOS is also used to generate the reference solution for this benchmark problem. The comparison of eigenvalues predicted by the two codes is illustrated in Table 11.1.

Table 11.1 Eigenvalue predicted by HELIOS and COMET

Core Averaged Burnup (GWd/tU)	HELIOS	COMET	Difference (pcm)
0 (Fresh)	1.15604	1.15981	377
2.5	1.0957	1.09663	93
5	1.07087	1.06960	-127
10	1.02375	1.02007	-368
15	0.98465	0.97968	-497
20	0.95078	0.94542	-536

As it can be seen from table 11.1, the eigenvalues predicted by COMET agree very well with those computed by HELIOS, with a maximum error of about 500 pcm. It should be pointed out that COMET is at least 4 orders of magnitude faster than HELIOS. The CPU running time for each COMET calculation is 2-3 seconds, while HELIOS takes about 20 hours for each burnup calculation.

## Task 12. Development of a thermal hydraulic module

### 1. Task Status and Significant Results

#### a. Task Summary

A new methodology for the accurate and efficient determination of steady state thermal hydraulic parameters for prismatic high temperature gas reactors is developed. Full core 3-D heat conduction calculations are performed at the individual fuel pin and assembly block levels. A simplified 1-D fluid model is developed to predict convective heat removal rates from solid core nodes. Finite volume discretization of energy, and momentum conservation equations are formed for each graphite and fuel unit cells, and then explicitly integrated in time. Using an initial temperature guess, iterations are performed until all local core temperatures stabilize and global convective heat removal matches heat generation. Assembly average block and fuel temperatures are then passed back to the neutronics module for pin power, and eigenvalue calculations.

Core temperature distributions are obtained with reduced computational cost over more highly detailed computational fluid dynamics codes by using efficient, natural models for the relevant thermal fluid and thermal transport phenomena. The thermal hydraulic module is parallelized using the distributed memory MPICH implementation of Message Passing Interface (MPI). Heat conduction and fluid calculations are divided equally among available processors. Typical steady state convergence is achieved after 18 hours on 8 processors.

#### b. Task Status/Progress

The thermal hydraulic module predicts whole core temperature, and mass flow distributions including bypass flow, using simple input files that contain all the necessary geometry and

thermal-fluid conditions. Results from the simulation are contained primarily in simple text files which can be read in to plotting software for visual inspection.

The level of detail of the developed method exceeds the current state-of-the-art for prismatic gas cooled reactor steady state thermal hydraulics. Using commonly assumed power profiles, and bypass gap dimensions, the predicted steady state temperature and mass flow distributions are comparable to those presented in the literature for either the MHTGR or GT-MHR reactor designs. Comparing the results from the developed method to CFD analyses in the literature shows that the temperature distribution within a single representative active fuel assembly block is similar. Differences can be primarily attributed to the single block CFD analyses which do not capture core environment mass flow effects. When comparing to more broad based, or system level codes, only the average graphite and fuel temperatures for a few assemblies can be compared. The average temperature results, for the peak assembly, in these cases are slightly higher than what is predicted by system level codes due to non-uniform mass flow in the core.

The development of the thermal hydraulic module is completed and results have been presented at two conferences with a journal paper expected.

### **Task 13. Implementation and test of coupled neutronics/thermal hydraulic calculations**

#### 1. Task Status and Significant Results

##### a. Task Summary

The thermal hydraulic and neutronic methods are coupled via pin fission density and block temperature data. An initial guess is made for the core temperature distribution, and the fission density profile of the core is determined for this set of temperatures. The fission density profile is given to the thermal fluids solver, which converts the data into power density figures, assuming a constant core power. A calculation proceeds to determine the core temperature profile based on the given power data. Average temperatures for the blocks are taken; for fuel blocks, both an average fuel temperature and an average moderator temperature is found, while for reflector blocks, only one value is taken to represent the block average. These results are given back to COMET for another core calculation. COMET takes the temperature data from the fluids solver, interpolates between temperature-dependent response function information in its data library, and determines the proper response function for each block, assuming the validity of linear interpolation between temperature points. Sensitivity analysis of the method is necessary in the near future to determine the legitimacy of this approach. The process continues until both the temperature data and the pin power profile converge to desired criteria.

##### b. Task Status/Progress

The coupled neutronics/thermal hydraulic method has been tested for a prismatic VHTR similar to the Modular High Temperature Gas Reactor (MHTGR) design. This is a 350 MWt core with prismatic graphite block structure and helium coolant. Coolant inlet temperature and pressure is 259°C and 6.39 MPa respectively. The core is composed of three inner reflector rings, surrounded by three active fuel rings, which are surrounded by two outer reflector block rings. Average coolant exit temperature is near 690°C. Principal results of the coupled analysis are described in the conference paper, Connolly et al. (2013). The following paragraphs summarize the results and key findings.

An initial temperature distribution equal to 350°C was assumed for the first neutronic iteration. The resulting pin fission densities were communicated to the thermal hydraulic module which proceeded to compute the graphite and fuel temperature distributions. A total of 9 coupled iterations (9 COMET iterations and 9 TH iterations) were performed with most COMET iterations completing in under an hour and the thermal hydraulic iterations under 18 hours. Convergence of the coupled method was verified by observing the change in eigenvalue and average temperature between iterations. The change in eigenvalue after 9 iterations was less than 10 pcm. The change in average core temperature after 9 iterations was less than 0.1°C.

The results from the converged coupled analysis indicated that power peaks near the inner and outer reflector block rings. Without any control rods inserted, the power peaks axially near the top of the reactor where the core is cooler. Fuel and graphite temperatures follow intuitively from this power distribution. Peak fuel temperatures are near 1050°C. Peak coolant temperatures exiting the reactor were near 922°C. The average temperature was lower due to cooler coolant exit temperatures from bypass flow in the reflector block regions.

## V. SUMMARY AND CONCLUSIONS

The objective of this research project is to develop a heterogeneous coarse mesh transport method/code for whole core calculations in 3-D hexagonal geometry for VHTR/NGNP prismatic reactors. In this method, a large heterogeneous eigenvalue (global) problem is decomposed into a set of smaller fixed source (local) problems without approximation and therefore with equal fidelity at all hierarchical levels (i.e., from the global (core) level to lower levels such as the fuel assembly). This method solves the global problem by iteratively using response functions to couple coarse meshes through interface partial currents. The whole core calculations are found to be highly accurate and very efficient.

A new thermal hydraulic method is developed for core-wide analysis of prismatic VHTR/NGNP reactors. The method allows for the complete solution of temperature and coolant mass flow distribution by solving quasi-steady energy balances for the discretized core. Assembly blocks are discretized into unit cells for which the average temperature of each unit cell is determined. Convective heat removal is coupled to the unit cell energy balances by a 1-D axial flow model. The coupled neutronics/thermal hydraulic method has been tested for a prismatic VHTR similar to the Modular High Temperature Gas Reactor (MHTGR) design.

A whole-core depletion method is developed to couple with COMET to provide transport theory analyses of reactor cores. This method is based on macro depletion techniques where the response coefficient library is generated as a function of assembly averaged burnup. Benchmark calculations have verified the method's high efficiency and accuracy.

In addition, a new time-dependent coarse-mesh transport model is rigorously developed. This new method relies on polynomial expansions of the solution to continuously couple coarse meshes in both space and time. Each mesh in the problem is completely characterized by a set of pre-computed response functions. By shifting the majority of the computation to the response function calculations, the actual core analysis can be performed very efficiently. Four example problems are used to demonstrate its high accuracy and efficiency.

Based on the encouraging results and efficiency obtained in this project it is recommended to extend this method to 3-D time-dependent problem. This will result in a highly accurate and efficient method for practical whole core calculations for prismatic VHTR design and analysis.

### Task/Milestone Status

Milestone/Task Description	Percent complete
1. Development of the RF generator in 2-D Hexagonal Geometry	100%
2. Development of the deterministic method in 2-D hexagonal geometry	100%
3. Development of a set of 2-D benchmark problems	100%
4. Development of 1-D time dependent RF generation method	100%
7. Development of a flux expansion method for 3-D hexagonal configurations	100%
8. Development of the RF generator for 3-D hexagonal geometry	100%
9. Development of the sweeping method for 3-D hexagonal geometry	100%
10. Development of a set of 3-D benchmark problems	100%
11. Development of a depletion module	100%

12. Development of a thermal hydraulic module	100%
13. Implementation and testing of coupled neutronics/thermal hydraulic/depletion calculations & benchmarking	100%
14. Reports, conference and journal papers	100%